

## Bifurcation Analysis of a Feedback System with Dead Zone and Saturation

By *M.G. Ortega, J. Aracil, F. Gordillo, and F.R. Rubio*

The control systems community is paying increasing attention to the complexity and richness of behavior that nonlinear systems can display [1]-[8]. These behaviors include self-sustained oscillations, which are out of the scope of the linear systems realm. Traditionally, control engineers have been concerned about local performance around the operating point, where the system can be approximated by a linear model. The presence of nonlinearities, however, must not be neglected to avoid global phenomena such as bifurcations or even chaos [9].

Nonlinear systems exhibit two main differences in behavior compared to linear systems: 1) they can have multiple equilibria, and 2) they can have limit sets more complex than limit points (for example, limit cycles and chaotic attractors [10]-[11]). These attractors are organized in attraction basins, giving rise to landscapes that are far more complex than those of linear systems, which are generically reduced to a single equilibrium point. To study these problems the tools supplied by the qualitative theory of nonlinear dynamical systems, and mainly bifurcation theory, could be used [12]-[13]. Bifurcation theory is concerned with the qualitative changes in the phase portrait of a system as a result of the birth or the disappearance of limit sets and their corresponding basins.

Many studies of bifurcations have been reported in the literature [12]-[13]. Some of the bifurcations, such as the Hopf or the saddle node, are well known. There is an analog to the saddle-node bifurcation for limit cycles that is quite interesting. This bifurcation happens when the coalescence of a stable limit cycle with an unstable one is produced. This phenomenon is represented in Fig. 1, which shows four phase portraits of the same system but for different values of a parameter  $\mu$  (known as the bifurcation parameter). The bifurcation parameter can change continuously, and the portraits shown in Fig. 1 are four samples of a continuous case. For the phase portrait of Fig. 1(d), a stable equilibrium point exists with an attraction basin (red zone) defined by an unstable limit cycle, which is surrounded by a stable one. The bifurcation is produced when the unstable limit cycle grows and/or the stable one decreases (in Fig. 1, evolution from (d) toward (c) and forward) until both coalesce (b) and disappear, and therefore only the equilibrium point remains (Fig. 1(a) is one example of the new situation). The bifurcation is produced for a value  $\mu_c$  of the bifurcation parameter (corresponding to phase portrait (b) in Fig. 1).

It should be noted that bifurcation analysis supplies a unifying framework to give an overall perspective of the behavior modes a system can display. Thus, all the behaviors of the system are organized within a single scheme. In this way, system designers have a powerful tool to understand, from a unified perspective, the complex effects associated with the nonlinearities of the system. It is also remarkable that bifurcation analysis can be implemented in some cases by frequency domain methods [7], [14], which are well known to control systems engineers.

In this article, the saddle-node bifurcation of periodic orbits is applied to the study of an elementary servomechanism with dead zone and actuator saturation to illustrate the statements in the previous paragraph. It will be shown that even if the behaviors are well known, the bifurcation analysis makes it possible to organize them in a single scheme. The stable and unstable limit cycles will be analyzed using the describing function method [15]-[18]. This method is approximate, but the error bounds for this approximation can be determined [19]. Some variants of the method can be applied to gain accuracy and even to detect multiple equilibria [20]. Furthermore, variants of the method exist that give rigorous results [17], [21] at the expense of some increased conservatism. Nevertheless, here we will show that the basic describing function method is sufficient to explain the behaviors.

The dc servomechanism used in this research may be modeled to a first approximation as a first-order system followed by an integrator. However, the emergence of periodic oscillations can be observed experimentally when a large disturbance is applied to the system output. Since this cannot be explained by linear theory, to justify such behavior it must be taken into account that the system also presents a

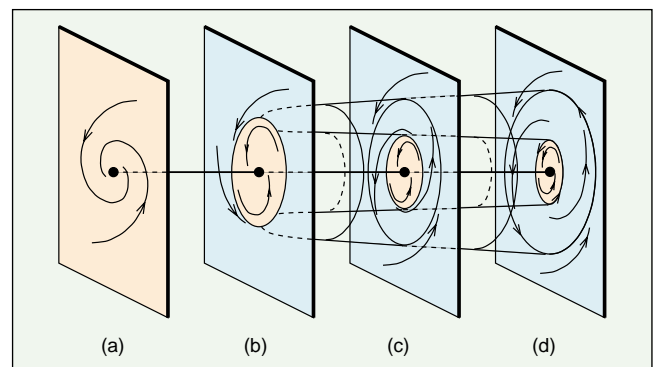


Figure 1. Description of the bifurcation in four phase portraits.

*Ortega (mortega@esi.us.es), Aracil, Gordillo, and Rubio are with the Departamento de Ingenieria de Sistemas y Automática, Escuela Superior de Ingenieros, Universidad de Sevilla, Spain.*

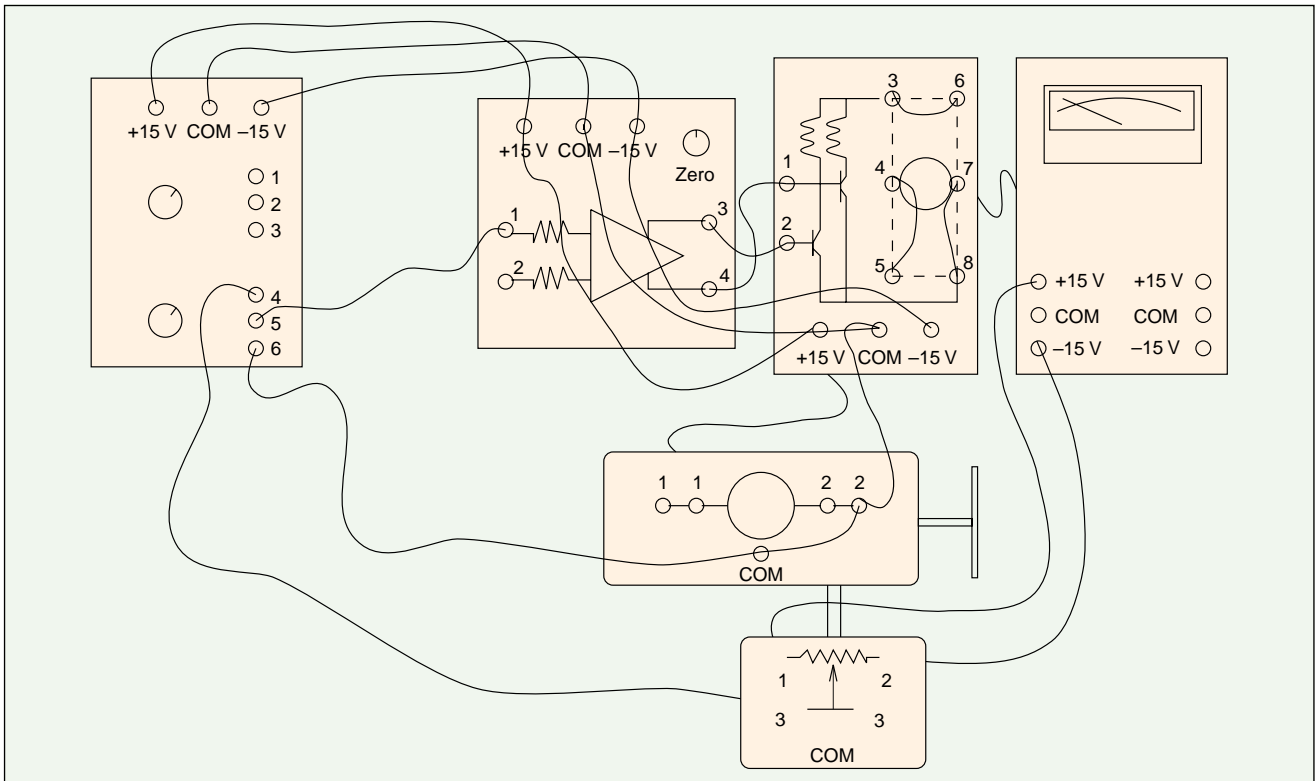


Figure 2. Connection diagram for the dc servomechanism.

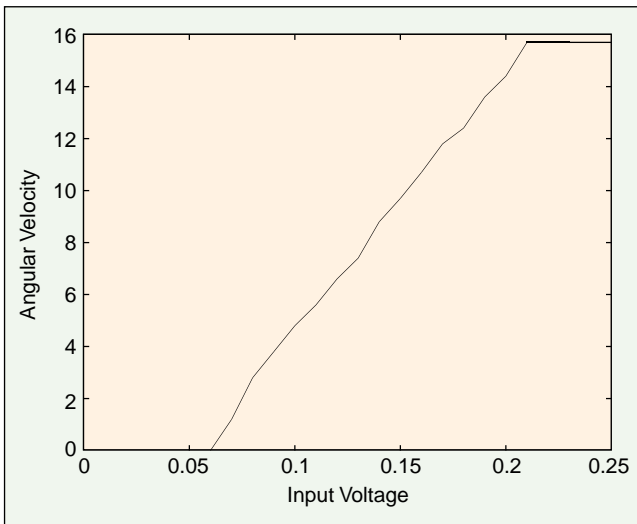


Figure 3. Static characteristic of the servomechanism for positive values of the input.

dead zone due to friction and a saturation zone because of the magnetic field saturation. The describing function method may be used to find the approximate amplitude and frequency of the periodic oscillations. It is necessary to keep in mind the high-frequency dynamics in the linear part of the model to explain the oscillations. The bifurcation parameter is simply the controller gain  $K_c$ , which allows us to state that limit cycles only appear when that gain has a suffi-

ciently high value. This will be made clear using a bifurcation diagram.

The main goal of this article is to present a global view of the behavior modes of the system. The approach we discuss does not attempt to strictly predict limit cycles, but rather to give an integrated view of the different behavior modes that have been detected experimentally on an elementary and well-known laboratory device. These behavior modes display state portraits where limit cycles (both stable and unstable) are present. The appearance of these limit cycles can be explained by the basic describing function method. It should be recalled that these behaviors cannot be explained with the tools supplied by linear dynamical systems theory.

This article is organized as follows: a description of the dc servomechanism is given first, including an analysis showing why the inclusion of high frequencies is necessary to explain the global behavior of the system. That is followed by an analysis of the system when the gain of the proportional controller varies. Experimental results are then presented, followed by conclusions.

### System Description

The system considered is a very popular servomechanism [22] used for student laboratory training. It is composed of a power supply, a preamplifier unit, a servo amplifier, an armature-controlled dc motor, a load unit inertia disk coupled to the motor, and an attenuator unit, which allows the load

unit position to be taken as the feedback signal. The connections diagram can be seen in Fig. 2, where the attenuator unit works as a proportional controller.

In accordance with this diagram, the input to the system to be controlled is the voltage applied to the preamplifier. The voltage provided by the potentiometer that measures the load position is the system output. In Fig. 3 the steady-state voltage, which represents the servomechanism angular velocity versus the system input voltage, is plotted for positive values of the input. It can be seen how the static characteristic of the system presents a dead zone with a threshold voltage of about 0.06 V. A quasi-linear zone follows it until a saturation zone is reached at a voltage of approximately 0.22 V. A graph of the corresponding nonlinearity placed at the input of the system is shown in Fig. 4.

An identification of the system from its temporal response to a step input can be performed to estimate its linear dynamic characteristic. A low-frequency model for this open-loop transfer function is given by

$$G(s) = \frac{100}{(1.5s+1)} \frac{6.25}{s}$$

The above expression has been separated into two parts: 1) a first-order system that represents the behavior of the servomechanism angular velocity given changes in the system input signal; and 2) an integrator with a proportional constant that is calculated experimentally with high accuracy. The latter relates the system output (the output voltage proportional to the angular position) to the angular velocity of the servomechanism. A comparison between theoretical (solid) and experimental (dashed) responses is shown in Fig. 5. As can be seen, the system is reasonably well identified, at least at low frequencies.

### High-Frequency Analysis

The resulting control diagram is shown in Fig. 6, where  $K_c$  represents the attenuator gain (less than or equal to one).

The describing function method can be used to study the oscillations of a nonlinear system [15], [17]-[18], [23]. It is well known that the condition for the existence of limit cycles is the following:

$$L(j\omega) = \frac{-1}{N(A,\omega)}$$

where  $L(s)$  is the transfer function of the linear part of the system and  $N(A,\omega)$  is the describing function of the nonlinearity. If this equation has a solution  $(A_0, \omega_0)$ , then a limit cycle with amplitude  $A_0$  and frequency  $\omega_0$  is predicted.

The open-loop transfer function of the system is

$$L(j\omega) = G(s)K_c$$

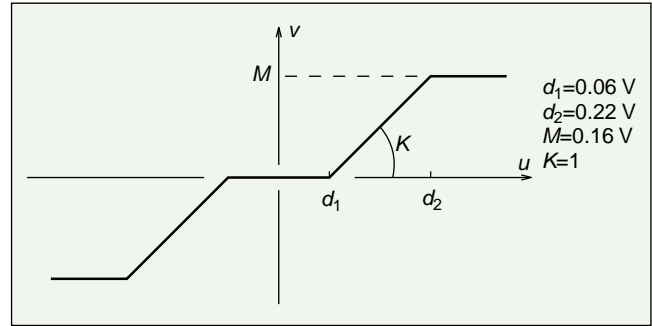


Figure 4. Description of the nonlinearity.

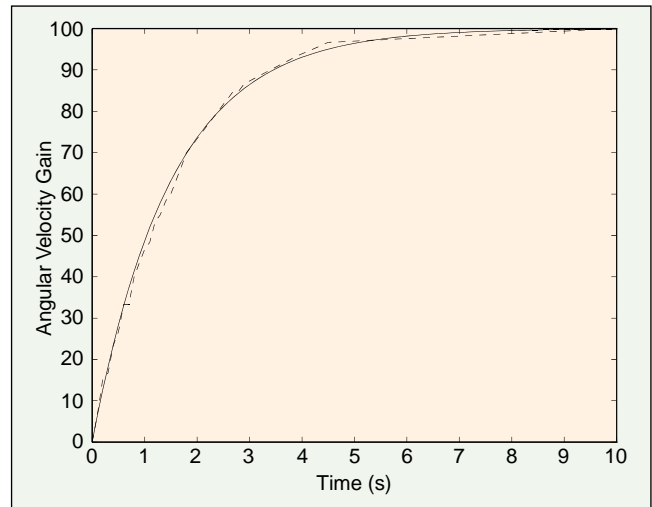


Figure 5. Dynamic characteristic of the servomechanism.

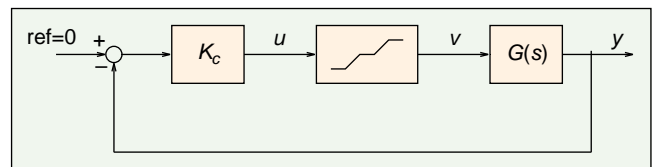


Figure 6. System structure with a proportional controller.

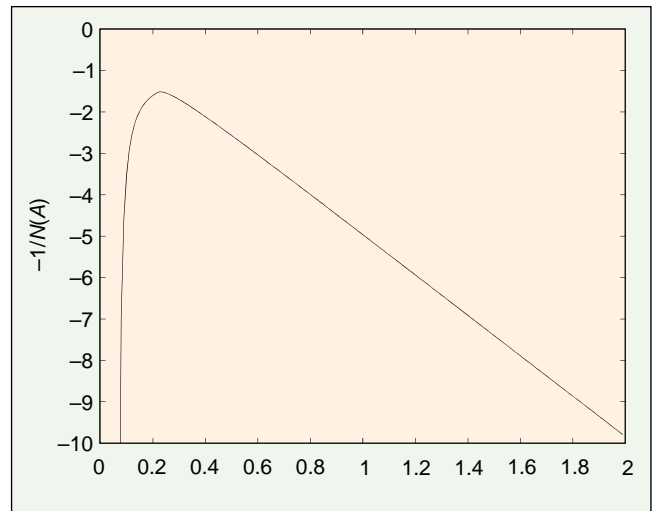


Figure 7. Plot of  $-1/N(A)$  versus  $A$ .

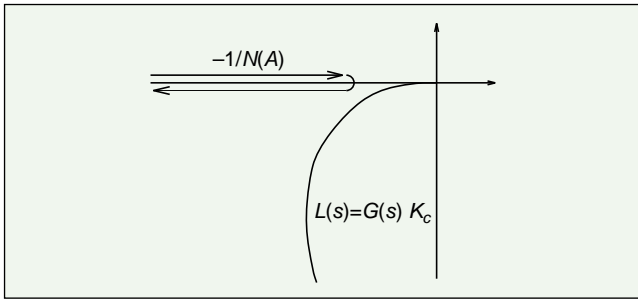


Figure 8. Diagrams of the describing and transfer functions.

while the describing function of its nonlinearity has the following expression [23]:

$$N(A) = \begin{cases} 0, & \text{if } 0 < A \leq d_1 \\ \frac{M}{d_2 - d_1} \left[ 1 - f\left(\frac{d_1}{A}\right) \right], & \text{if } d_1 < A \leq d_2 \\ \frac{M}{d_2 - d_1} \left[ f\left(\frac{d_2}{A}\right) - f\left(\frac{d_1}{A}\right) \right], & \text{if } d_2 < A \end{cases}$$

where

$$f(x) = \frac{2}{\pi} \left( \arcsin x + x \sqrt{1-x^2} \right).$$

This describing function does not depend on the frequency and is always real and greater than or equal to zero. The negative of its inverse,  $-1/N(A)$ , is shown in Fig. 7. It starts from  $-\infty$  for very low amplitudes until it reaches a negative maximum. After that, it tends again to  $-\infty$  for very high amplitudes.

The Nyquist plots of  $L(s)$  and  $-1/N(A)$  are drawn in a polar diagram in Fig. 8. Although the graph of  $-1/N(A)$  is on the real axis, this graph has been plotted off of it to display its shape. It can be seen that the graphs of  $L(s)$  and  $-1/N(A)$  do not intersect each other since the model is second order, and therefore the open-loop transfer function can only cut the real axis at the origin and at frequencies tending toward infinity.

The fact that there is no intersection between the two graphs implies that there is no theoretical possibility of existence of limit cycles according to the describing function method. However, it actually happens that for high values of  $K_c$ , if the load position in the equipment is disturbed enough, the system presents a stable limit cycle.

From that it is deduced that the system model is not accurate enough to explain the real system behavior. Therefore, the transfer function needs to be modified to take into account the high-frequency dynamics. A new high-frequency pole whose time constant is estimated at 0.003 s is added to the transfer function, obtaining the following expression:

$$G(s) = \frac{100}{(1.5s+1)(0.003s+1)} \frac{6.25}{s}.$$

The new pole hardly affects the time response of Fig. 5 but has important consequences regarding the analysis of limit cycles. Thus, the intersection between  $L(s)$  and  $-1/N(A)$  is now possible with this new expression. This is made clear in Fig. 9, where two points can be emphasized. The first is that  $L(s)$  intersects  $-1/N(A)$  twice with the same frequency but different amplitudes, which yields the existence of two limit cycles. In addition, the intersections have different directions, which implies that one of the limit cycles (the one with higher amplitude) is stable and the other is unstable. The second point is that the intercept between the two curves is quite plane, which implies that the conclusions obtained from the describing function method are not accurate, but they are valid as qualitative results [19].

#### Survey of the System Behavior Against $K_c$ Variations

The experimental detection of the limit cycles was performed for a specific value of the constant of the proportional controller. A survey of different behavior modes of

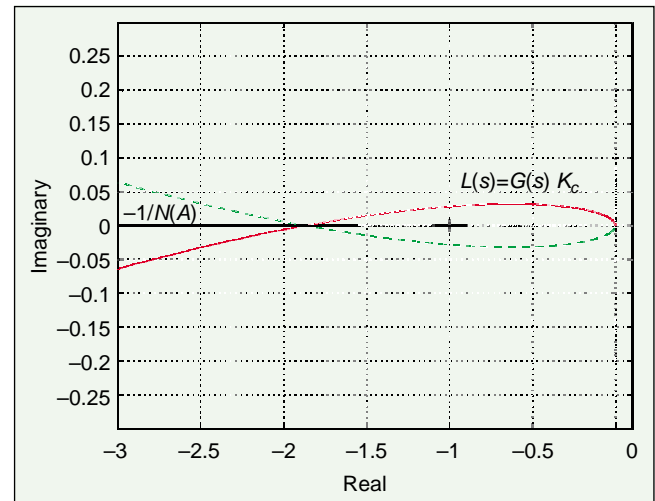


Figure 9. Diagrams of the describing and augmented transfer functions ( $K_c = 1$ ).

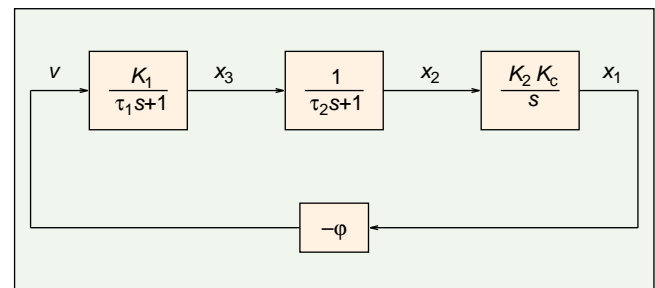


Figure 10. Diagram of the system expressed in state-space variables.

the system that can appear as a result of varying  $K_c$  is made in this section. The first step is to make a state-space realization of the system. The open-loop system can be expressed as

$$L(s) = \frac{K_1}{(\tau_1 s + 1)(\tau_2 s + 1)} \frac{K_2 K_c}{s}$$

where  $K_1=100$ ,  $K_2=6.25$ ,  $\tau_1=15$ , and  $\tau_2=0.003$ . The closed-loop system can be depicted by means of a block diagram, as in Fig. 10, where  $\phi(\cdot)$  is the nonlinearity.

The system dynamics of Fig. 10 are governed by the following equations:

$$\begin{bmatrix} \dot{x}_1 \\ \dot{x}_2 \\ \dot{x}_3 \end{bmatrix} = \begin{bmatrix} f_1(x_1, x_2, x_3) \\ f_2(x_1, x_2, x_3) \\ f_3(x_1, x_2, x_3) \end{bmatrix} = \begin{bmatrix} 0 & K_2 K_c & 0 \\ 0 & -1/\tau_2 & 1/\tau_2 \\ 0 & 0 & -1/\tau_1 \end{bmatrix} \begin{bmatrix} x_1 \\ x_2 \\ x_3 \end{bmatrix} - \begin{bmatrix} 0 \\ 0 \\ \phi(x_1) K_1 / \tau_1 \end{bmatrix},$$

where  $-\phi(\cdot)$  represents the negative feedback of the nonlinearity.

It should be noted that state  $x_2$  corresponds to the servomechanism velocity whereas state  $x_1$  is the load angular position multiplied by the proportional constant of the controller.

### Equilibrium Points and Their Stability

The temporal derivatives of the state variables should be equated to zero to find the equilibrium points of the system. Setting  $\dot{x}_i$  ( $i=1,2,3$ ) equal to zero yields

$$\begin{aligned} \dot{x}_1=0 &\Rightarrow K_2 K_c x_2^e = 0 &\Rightarrow x_2^e = 0 \\ \dot{x}_2=0 &\Rightarrow -x_2^e / \tau_2 + x_3^e / \tau_2 = 0 &\Rightarrow x_3^e = 0 \\ \dot{x}_3=0 &\Rightarrow -x_3^e / \tau_1 - K_1 / \tau_1 \phi(x_1) = 0 &\Rightarrow \phi(x_1) = 0 \\ &&\Rightarrow -d_1 \leq x_1^e \leq d_1. \end{aligned}$$

According to the above conditions, equilibrium points should have zero velocity ( $x_2^e = 0$ ); moreover, the absolute value of the angular position multiplied by the controller constant should not exceed the dead zone threshold ( $|x_1^e| \leq d_1$ ). This yields a band of equilibrium points (i.e., the equilibrium points are not isolated).

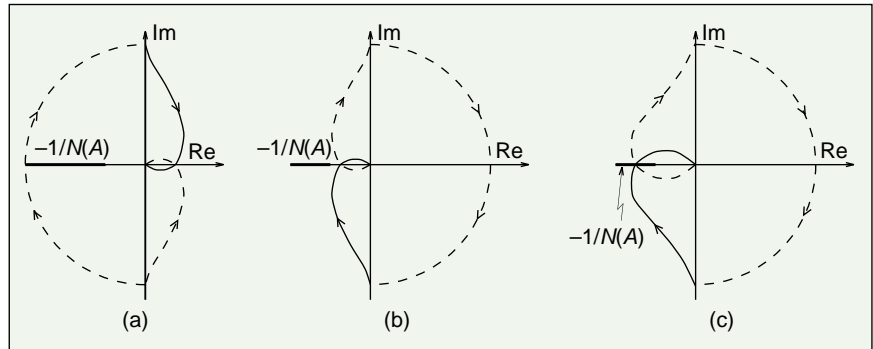


Figure 11. Nyquist plot of  $L(s)$ : (a)  $K_c < 0$ ; (b)  $K_c > 0$  and small; (c)  $K_c > 0$  and large.

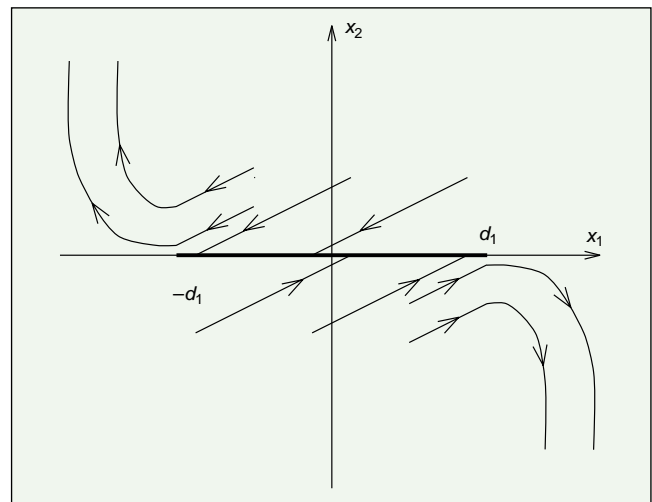


Figure 12. State-space diagram:  $x_1$  versus  $x_2$  for negative values of  $K_c$ .

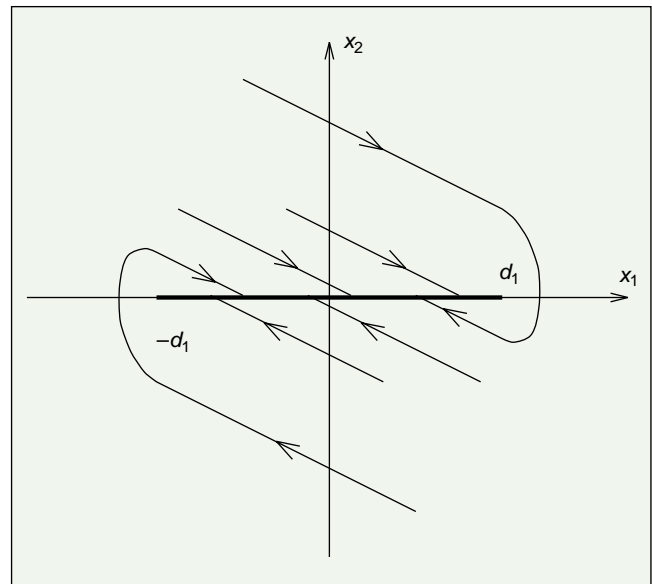


Figure 13. State-space diagram:  $x_1$  versus  $x_2$  for positive and small values of  $K_c$ .

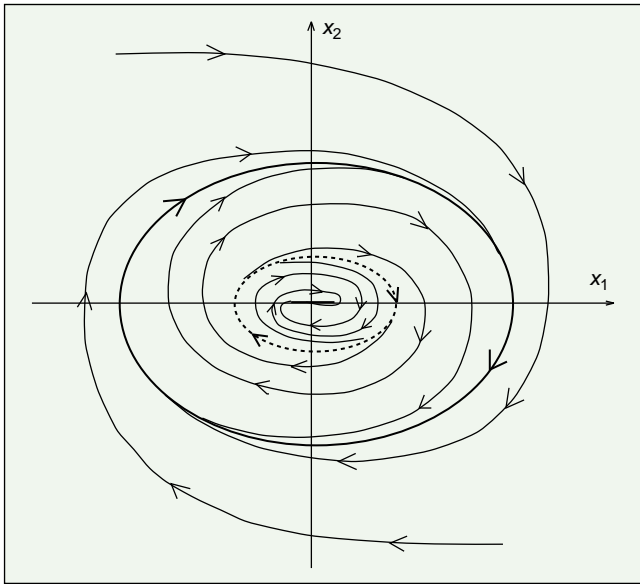


Figure 14. State-space diagram:  $x_1$  versus  $x_2$  for high values of  $K_c$ .

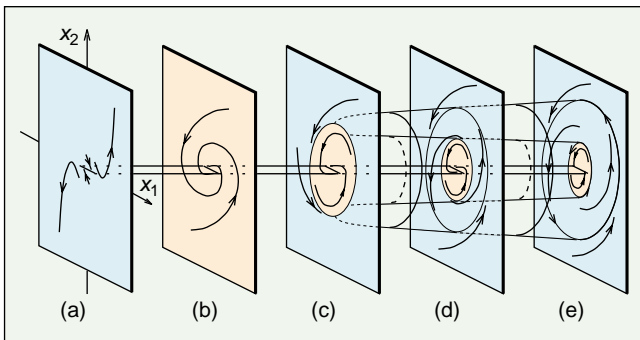


Figure 15. Description of the bifurcation of the dc servomechanism in five portraits (red: stable region; blue: unstable region).

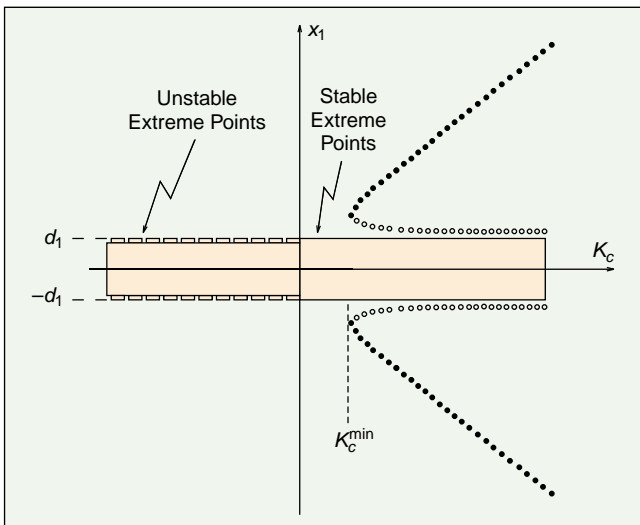


Figure 16. Bifurcations diagram.

The Jacobian matrix for this system is the following:

$$J(x_i) = \frac{\partial f_i}{\partial x_j} = \begin{bmatrix} 0 & K_2 K_c & 0 \\ 0 & -1/\tau_2 & 1/\tau_2 \\ d\varphi(x_1)/dx_1 & 0 & -1/\tau_1 \end{bmatrix}$$

At this point, we must separate the equilibrium points into two sets: an open set of equilibrium points with  $|x_1^e| < d_1$  and the isolated extreme points (i.e.,  $|x_1^e| = d_1$ ).

Particularizing  $J(x_i^e)$  for the equilibrium points of the first set and keeping in mind that

$$-d_1 < x_1^e < d_1 \Rightarrow \varphi(x_1) = 0 \Rightarrow d\varphi(x_1)/dx_1 = 0,$$

it can be seen that for these points

$$J(x_i^e) = \begin{bmatrix} 0 & K_2 K_c & 0 \\ 0 & -1/\tau_2 & 1/\tau_2 \\ 0 & 0 & -1/\tau_1 \end{bmatrix}$$

Furthermore, this Jacobian is not an approximation; rather it is exact in the neighborhood of each equilibrium, since in this neighborhood  $\varphi=0$  and the system is linear. The eigenvalues of this matrix are  $\lambda_1 = -1/\tau_1 < 0$ ,  $\lambda_2 = -1/\tau_2 < 0$ , and  $\lambda_3 = 0$ . When one eigenvalue is zero, the phase portrait is in some sense degenerate; that is, the system has an equilibrium subspace rather than an equilibrium point. Since two of the eigenvalues are negative and the third one is zero, the system is stable but not asymptotically stable. There is a direction in the state space, the one associated with the zero eigenvalue, that is neutral.

The above statements cannot be valid for the isolated extreme points of equilibrium, however, since the derivative of the nonlinearity does not exist at these points. Thus, another method must be used to analyze the stability of the extreme points of the band. For this case, some considerations of the describing function analysis are applied to clarify the stability of these points.

It is well known that in the describing function analysis, the conventional frequency-response analysis is modified so that the entire  $-1/N(A,\omega)$  locus becomes a locus of critical points. Thus, the relative location of the  $-1/N(A,\omega)$  locus and the Nyquist plot of  $L(s)$  provides the stability information.

To determine the stability of the system, the  $-1/N(A,\omega)$  locus and the  $L(j\omega)$  locus are plotted. If all the poles and zeros of  $L(s)$  lie on the left half of the  $s$ -plane, including the  $j\omega$  axis (as is the case of the system under consideration), the criteria for stability say that:

- If the  $-1/N(A,\omega)$  locus is not enclosed by the  $L(j\omega)$  locus, then the system is stable and there is no limit cycle at the steady state.

- If the  $-1/N(A, \omega)$  locus is enclosed by the  $L(j\omega)$  locus, then the system is unstable.
- If the  $-1/N(A, \omega)$  locus and the  $L(j\omega)$  locus intersect, then a limit cycle is predicted for the system output.

It is easy to see that, in contrast to the continuous set of equilibrium points, the stability of the extreme points depends on the value of  $K_c$ . As will be explained in more detail in the next section, here we can distinguish three cases, depending on the value of the controller constant:

1. *Negative values of  $K_c$  (positive feedback):* In this case, given a value of  $A$ , it can be considered that the Nyquist plot of  $L(s)$  encircles the point  $-1/N(A)$ , provided that a sufficiently small radius is selected to surround the pole  $s=0$  [Fig. 11(a)]. Therefore, the extreme equilibrium points are unstable. This case, however, is unrealistic from a control engineering viewpoint. It is included only for the sake of mathematical completeness.
2. *Small and positive values of  $K_c$ :* In this case, there is no intersection between the  $-1/N(A)$  locus and the  $L(j\omega)$  locus [Fig. 11(b)]. Thus, the extreme equilibrium points are stable under these conditions.
3. *Large and positive values of  $K_c$ :* In this case, there are two intersection points between the  $-1/N(A)$  locus and the  $L(j\omega)$  locus [Fig. 11(c)]. As will be seen in the next section, this implies the existence of two limit cycles, the first of them unstable and the second one stable. Since the nearest limit cycle to the equilibrium point is unstable, we can conclude that the extreme equilibrium points are also stable under these conditions.

### Limit Cycles

The crossing points between  $-1/N(A)$  and the Nyquist plot of  $L(s)$  are sought to predict limit cycles. As stated earlier,  $-1/N(A)$  is real and negative (Fig. 7), which implies that the intercepts between the open-loop transfer function and the negative real axis must be studied. Taking into account that  $K_c$  is a real constant, the intersection points between this function and the real negative axis have the form

$$L(j\omega_{180}) = K_c G(j\omega_{180}) = -K_c K,$$

where

$$K = \frac{K_1 K_2 \tau_1 \tau_2}{\tau_1 + \tau_2} = \text{constant}.$$

According to the above expression, and since  $-1/N(A)$  has a negative maximum, no limit cycle exists for low values of  $K_c$  [see Fig. 11(b)]. If the value of  $K_c$  increases, it reaches a threshold ( $K_c^{\min} = \gamma/K \approx 0.8087$ ) where  $\gamma$  is the absolute value of the negative maximum of  $-1/N(A)$  at which the transfer function intersects  $-1/N(A)$ . At this point, two limit cycles

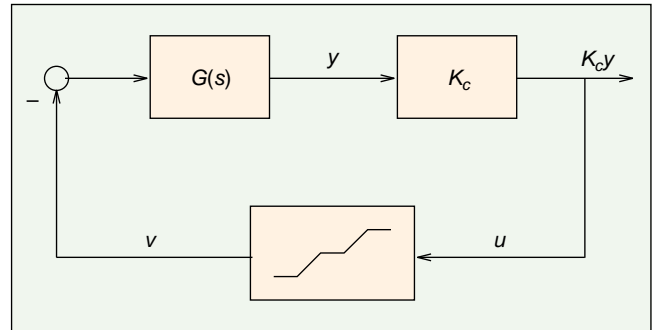


Figure 17. Control scheme used to study the bifurcations of the system.

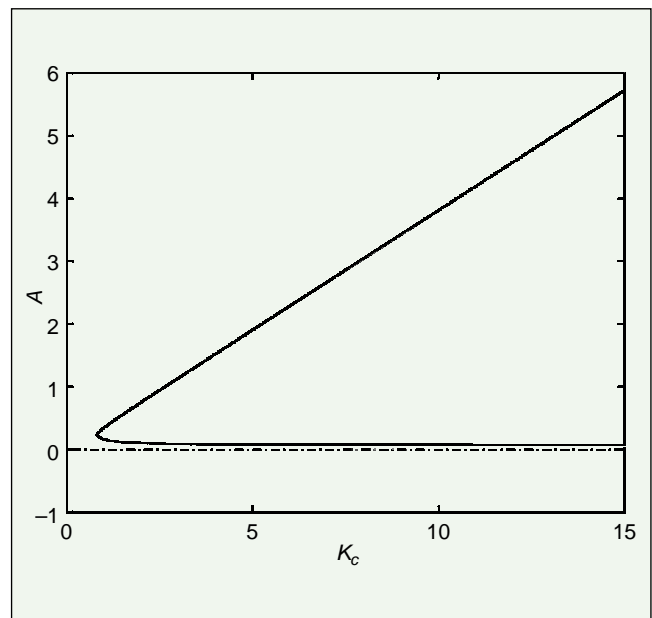


Figure 18. Amplitude of  $x_1$  in the limit cycles versus  $K_c$ .

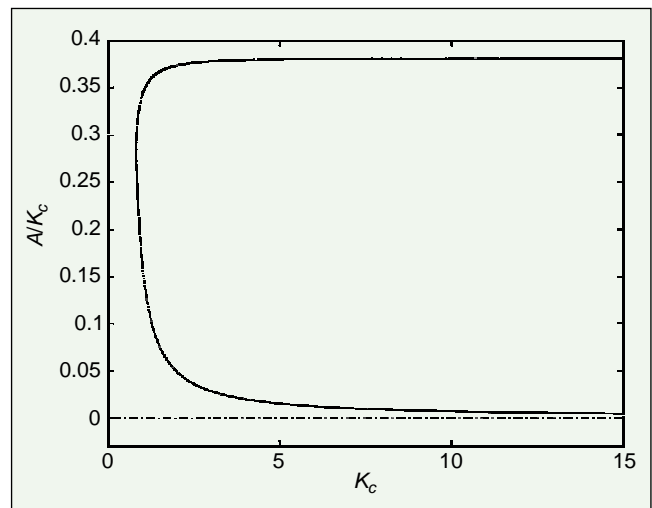


Figure 19. Amplitude of the limit cycles of the angular position versus  $K_c$ .

appear, one of them unstable and the other one stable. It must be emphasized that the frequency at which  $L(j\omega)$  intersects the real axis is constant and has a value of  $\omega_{180} = 14.91$  rad/s. This will be the frequency of oscillation of all the limit cycles that may appear. Following the same reasoning as in the “System Description” section, it can be concluded that the limit cycle with highest amplitude is stable and the one with the smallest amplitude is unstable.

According to these results, if  $K_c$  is greater than the threshold value, the stable equilibrium point has a limited attraction basin. Therefore, disturbances cause different behaviors depending on their magnitudes. If the disturbance is small, the system evolves toward the stable equilibrium point. On the other hand, if the disturbance is large

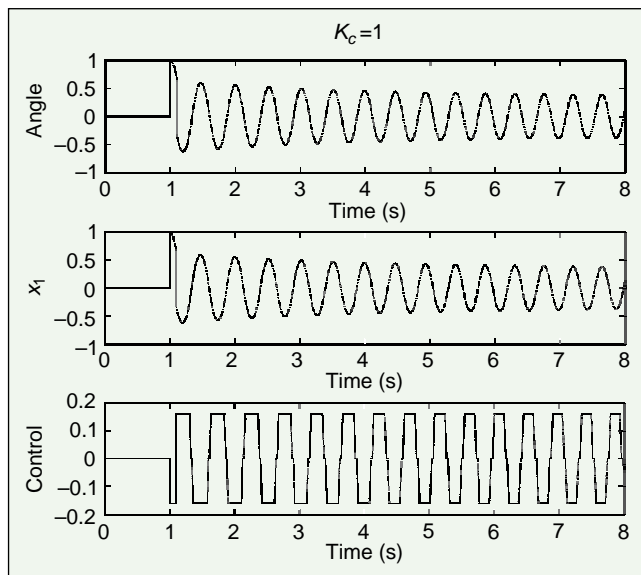


Figure 20. Simulation results for the system with  $K_c=1$ .

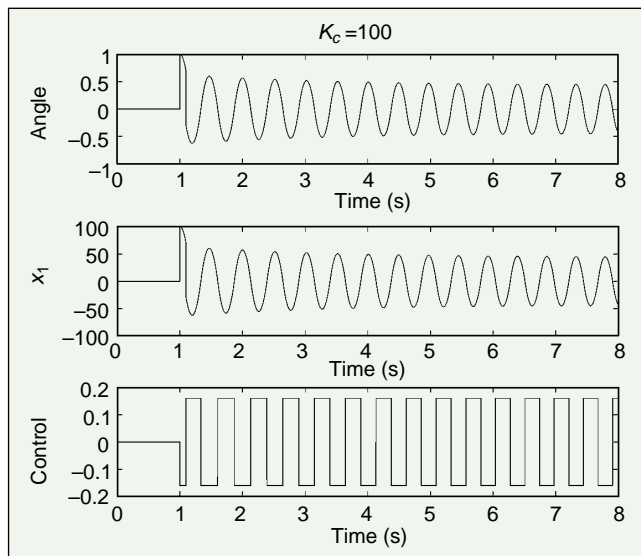


Figure 21. Simulation results for the system with  $K_c=100$ .

enough, the system leaves the attraction basin and evolves toward the stable limit cycle, which has greater amplitude than the unstable one.

In addition, as shown in the previous section, there are no limit cycles for negative values of  $K_c$  because there are no finite intersection points between  $L(j\omega)$  and  $-1/N(A)$ .

### Bifurcation Analysis

Since the system behavior shows qualitative changes when the parameter  $K_c$  varies, it is interesting to perform a bifurcation analysis of the system with regard to this parameter.

As shown in the previous section, the equilibrium points can be separated into two sets. The first is composed of the equilibrium points that have  $|x_1| < d_1$  (the inner points of the band). These equilibrium points have neutral stability independent of the value of the parameter  $K_c$ .

The stability of the extreme points of the band changes, however, depending on the value of the parameter  $K_c$ . Thus, for negative values of  $K_c$  these equilibrium points are unstable. It is also known that there are no limit cycles for these values of  $K_c$ . The system behavior under these conditions is shown in Fig. 12 in a qualitative diagram of states, where states  $x_1$  versus  $x_2$  are depicted.

On the other hand, the extreme equilibrium points are stable for positive values of the parameter  $K_c$ , but the system behavior varies depending on the magnitude of this parameter. In particular, as discussed in a previous section, no limit cycles exist if the value of  $K_c$  is small. The system behavior under these conditions is depicted in a state diagram in Fig. 13.

The fact that a change in the stability of some equilibrium points has been produced, varying the parameter  $K_c$ , is a first change in the phase portrait, which occurs when the value of  $K_c$  becomes zero.

In addition, another bifurcation (a saddle-node bifurcation of periodic orbits) appears when the value of the parameter  $K_c$  reaches a value  $K_c^{\min}$ . For values of  $K_c$  greater than  $K_c^{\min}$ , there are two limit cycles surrounding the band of stable equilibrium points. Under these conditions, the system evolves as shown in the state diagram in Fig. 14.

Figs. 12, 13, and 14 represent qualitatively different behavior modes of the system as parameter  $K_c$  varies. These different behaviors can be unified in a single scheme, as presented in Fig. 15.

The behavior of the system for high values of  $K_c$  is presented in Fig. 15(e), where the band of equilibrium points is stable, as is shown in Fig. 14. As the parameter  $K_c$  decreases [Fig. 15(d)], the amplitude of the unstable limit cycle increases while the amplitude of the stable one decreases until parameter  $K_c$  reaches the value of  $K_c^{\min}$  [Fig. 15(c)]. At this value of  $K_c$ , the coalescence of the limit cycles is produced, giving rise to their extinction. For values of  $K_c$  less than  $K_c^{\min}$  but positive [Fig. 15(b)], the band of equilibrium points re-

mains stable and the amplitude of its attraction basin is infinite, since there are no limit cycles surrounding it (phase portrait of Fig. 13). Finally, when  $K_c$  reaches a negative value [Fig. 15(a)], the extreme equilibrium points of the band become unstable. This implies that if a small disturbance causes the system to evolve toward the outside of the zone  $|x_1| \leq d_1$ , the state variables will evolve away indefinitely from their equilibrium values (recall Fig. 12). It is worth noting how the conventional saddle-node bifurcation of Fig. 1 has been transformed into a more complex one, in this case due to the dead zone.

It is very interesting to note that in the saddle-node bifurcation of periodic orbits, two limit cycles are born when  $K_c$  varies from the one of part b to that of part d in Fig. 15. The emergence of these limit cycles has two main differences with respect to the better-known Hopf bifurcation: 1) the limit cycles emerge with amplitude different from zero, and 2) the stability of the equilibrium point does not change. These two differences have an important consequence for the control engineer: a local analysis around the equilibrium point would not detect the emergence of the limit cycles and consequently the loss of global stability. This is why it is necessary to use a global (even if, in this case, approximate) method, such as the describing function method, to detect such a bifurcation.

The bifurcation scheme of Fig. 15 is usually represented on a bidimensional plane, as shown in Fig. 16. This last bifurcations diagram summarizes the dynamic behavior of a system in only one scheme. In this case, it is useful to represent state  $x_1$  versus  $K_c$  (see Fig. 16).

We can see that a band of equilibrium points exists whose inner points have neutral stability and whose extreme points are stable for positive values of  $K_c$  and unstable for negative (but unrealistic) values of this constant.

On the other hand, we can also see that a bifurcation appears when the value of the controller constant is equal to a minimum value  $K_c^{\min}$ . Starting from this value, there are two limit cycles surrounding the band of stable equilibrium points. Therefore, if a disturbance is large enough, the system evolves from one of these points, crossing the unstable limit cycle, and enters the attraction field of the stable limit cycle, where it remains, oscillating indefinitely (see Fig. 14).

It should be noted that the describing function method is not strictly used to study bifurcations. In fact, we are not interested in the bifurcation point itself. The saddle-node bifurcation is used as a generic archetype to give a unified view of how the transition between different state portraits is produced. Therefore, the contribution of the paper is not the prediction of a bifurcation, but a method for obtaining a unified framework for system behaviors.

#### Remarks

To interpret the physical consequences of the diagram in Fig. 16, the relationship between the state variables and the

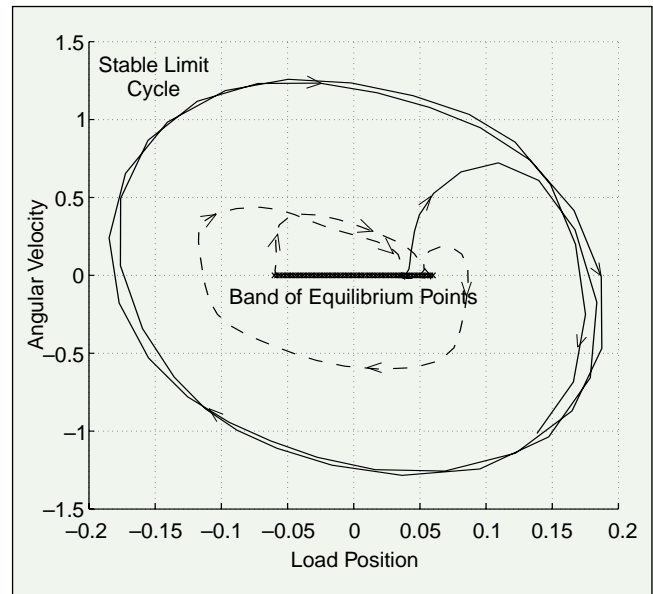


Figure 22. Experimental state-space diagram:  $x_1$  versus  $x_2$  for  $K_c=1$ .

load angular position must be considered. As stated earlier, state  $x_2$  corresponds to the angular velocity of the servomechanism, whereas state  $x_1$  is the load angular position multiplied by  $K_c$ . This is because the system studied is the one shown in Fig. 17, whereas the physical system corresponds to the scheme in Fig. 6. These two schemes are equivalent since the reference is zero.

The amplitude of state  $x_1$  should be divided by the chosen value of  $K_c$  to find the physical measurable magnitude of the load angular position. The amplitude of  $x_1$  in the limit cycle versus values of  $K_c$  is plotted in Fig. 18. It can be seen that for large values of  $K_c$ , the amplitude of the stable limit cycle grows linearly while the amplitude of the unstable one tends toward the threshold value of the dead zone  $d_1$ .

Consequently, the amplitude of the angular position in the stable limit cycle will remain constant while the amplitude of the unstable one will tend toward zero for values of  $K_c$  tending toward infinity (Fig. 19). This agrees with the usual loss of robustness when the gain of the controller is high in linear control theory. However, results based on linear theory can only state that the system behavior becomes unstable when small disturbances are applied. It is clear that the farther the system is from the bifurcation point, the more robust it is. This shows the relevance of bifurcation analysis, since it explains not only the local behavior (as in the case of linear theory applied to nonlinear systems), but also the system global behavior.

In addition, the fact that the amplitude of the stable limit cycle is constant for high values of  $K_c$  agrees with what is expected from physical experiments, because the control signal given by a proportional controller should be approximately the same for any high value of  $K_c$  due to the

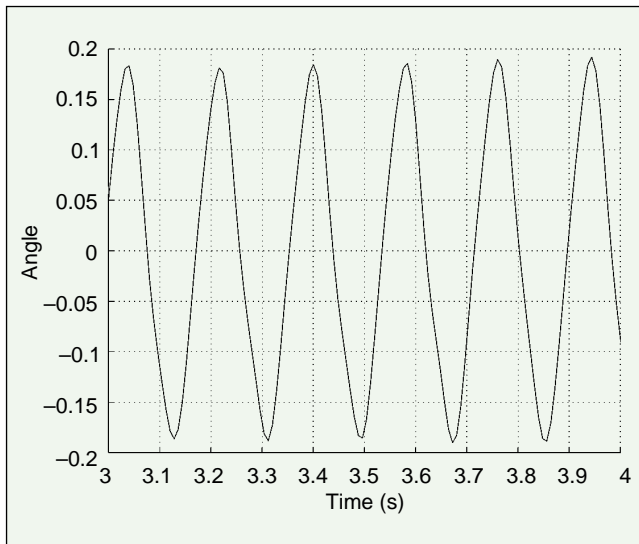


Figure 23. Experimental limit cycle of the load position for  $K_c=1$ .

saturation. Simulation results for values of  $K_c$  equal to 1 and 100 are shown in Figs. 20 and 21. It can be seen that the evolution of the angular position is very similar, since the control signals are almost the same. Obviously, the system output used for studying the dynamic behavior, that is,  $x_1$ , does not have similar values.

Finally, this example shows the ambiguity of the concept of stability as used by the control community. The system is bounded-input, bounded-output stable for values of  $K_c$  greater than zero, but such specification of stability is poor for the practical engineer, as it can correspond to two different, although bounded, behaviors: one oscillating and the other steady. Furthermore, the steady-state behavior is not asymptotically stable.

### Experimental Results

Several tests have been carried out on the dc servomechanism to obtain experimental results. The load position and angular velocity have been measured for a value of the parameter  $K_c$  equal to one, which implies that the state-space variable  $x_1$  coincides with the load position.

Some experimental results are presented in Fig. 22 in a state-space diagram plotting load position versus angular velocity ( $x_1$  versus  $x_2$ ). In this figure, we can distinguish experiments (dashed trajectories) starting from an equilibrium point with small disturbance applied to the load; the system evolves until it reaches another equilibrium point. Also plotted in this figure is another experiment where a sufficiently large disturbance is applied to the load to cause the system to cross the unstable limit cycle and evolve into the stable one (continuous trajectory). It must be noted that the

value of  $K_c$  chosen to carry out these experiments ( $K_c=1$ ) is greater than the minimum value of  $K_c$  necessary to allow the existence of periodic oscillation in the system ( $K_c^{\min} \approx 0.8087$ ), but close to it. It should also be noted that although the order of the system considered is three, the experimental results are presented in a bidimensional figure. This explains why there are some intersections between the various trajectories in Fig. 22.

A graph of the load position oscillation obtained experimentally for  $K_c=1$  is shown in Fig. 23. The amplitude of the oscillation is 0.19 and its frequency is 34.68 rad/s. The amplitude and frequency of this oscillation computed from the describing function method are 0.34 and 14.31 rad/s, respectively, whereas the simulated results (see the first graph of Fig. 20) are 0.37 and 18.30 rad/s, respectively. These discrepancies are due to the intercept between the transfer function and the describing function being quite plane, which implies that the results obtained from the describing function method are not accurate, as stated earlier. Nevertheless, what is relevant for the control engineer is not the numerical accuracy but the qualitative detection of abnormal phenomena, such as the occurrence of oscillations or the possibility of an unstable limit cycle that bounds the attraction basin, leading to the loss of global stability. Such types of problems are highly relevant for control engineers, and the qualitative analysis based on describing function methodology developed in this paper has resulted in a classification of the behavior modes the system can display.

### Conclusions

An experimental example has been presented showing how nonlinearities affect the dynamic behavior of a dc servomechanism controlled by a proportional controller. The analysis has been developed using tools supplied by classical methods for feedback system analysis based on the describing function method. The case studied is a very good and simple example of a feedback system where a saddle-node bifurcation of periodic orbits occurs. This bifurcation is very interesting because it explains the coexistence of a stable equilibrium at the operating point with a stable limit cycle for large perturbations. The major advantage of the bifurcation analysis developed is that it supplies a single unified framework for representing all the different behavior modes the system can display. Finally, these results have been tested using laboratory equipment.

### Acknowledgments

The authors wish to acknowledge CICYT for its support for projects TAP98-0541 and TAP97-0553. Likewise, the authors appreciate the comments by Enrique Ponce on a draft of this article. They also acknowledge the many helpful sugges-

tions by reviewers and editors that have been incorporated into the manuscript.

## References

- [1] E.H. Abed, H.O. Wang, and A. Tesi, "Control of bifurcations and chaos," in *The Control Handbook*, W.S. Levine, Ed. Piscataway, NJ: IEEE, 1996, pp. 951-966.
- [2] J. Alvarez and E. Curiel, "Bifurcations and chaos in a linear control system with saturated input," *Int. J. Bifurcation Chaos*, vol. 7, no. 10, pp. 1811-1821, 1997.
- [3] J. Alvarez, E. Curiel, and F. Verduzco, "Complex dynamics in classical control systems," *Syst. Contr. Lett.*, vol. 31, pp. 277-285, 1997.
- [4] J. Aracil, K.J. Aström, and D. Pagano, "Global bifurcations in the Furuta pendulum," in *Proc. IFAC Nonlinear Control Systems Design*, Enschede, The Netherlands, 1998, pp. 37-41.
- [5] J. Aracil, F. Gordillo, and T. Álamo, "Global stability analysis of second-order fuzzy control systems," in *Advances in Fuzzy Control*, R. Palm, D. Driankov and H. Hellendorn, Eds. New York: Springer-Verlag, 1998.
- [6] J. Llibre and E. Ponce, "Global first harmonic bifurcation diagram for odd piecewise linear control systems," *Dynam. Stability Syst.*, vol. 11, no. 1, pp. 49-88, 1996.
- [7] J. Moiola and G. Chen, *Hopf Bifurcation Analysis: A Frequency Domain Approach*. Singapore: World Scientific, 1996.
- [8] D. Pagano, E. Ponce, and J. Aracil, "Bifurcations analysis of low-order nonlinear control systems with a delay," in *Proc. Int. Conf. Control of Oscillations and Chaos*, St. Petersburg, FL, 1997, pp. 478-483.
- [9] G. Chen and X. Dong, *From Chaos to Order: Methodologies, Perspectives and Applications*. Singapore: World Scientific, 1998.
- [10] A.H. Nayfeh and B. Balachandran, *Applied Nonlinear Dynamics*. New York: Wiley, 1995.
- [11] S.H. Strogatz, *Nonlinear Dynamics and Chaos*. Reading, MA: Addison-Wesley, 1995.
- [12] J.K. Hale and H. Koçak, *Dynamics and Bifurcations*. New York: Springer-Verlag, 1991.
- [13] Y.A. Kuznetsov, *Elements of Applied Bifurcation Theory*. New York: Springer-Verlag, 1995.
- [14] M. Basso, R. Genesio, and A. Tesi, "A frequency method for predicting limit cycle bifurcations," *Nonlinear Dynam.*, vol. 13, pp. 339-360, 1997.
- [15] P.A. Cook, *Nonlinear Dynamical Systems*, 2nd. ed. Englewood Cliffs, NJ: Prentice-Hall, 1994.
- [16] J.K. Hedrick, "Nonlinear system response: Quasi-linearization methods," *A.S.M.E. Nonlinear System Analysis and Synthesis*, chap. 4, vol. 1, pp. 97-124, 1978.
- [17] H.K. Khalil, *Nonlinear Systems*, 2nd ed. Englewood Cliffs, NJ: Prentice-Hall, 1996.
- [18] M. Vidyasagar, *Nonlinear Systems Analysis*, 2nd ed. Englewood Cliffs, NJ: Prentice-Hall, 1993.
- [19] A.R. Bergen, L.O. Chua, A.I. Mees, and E.W. Szeto, "Error bounds for general describing function problems," *IEEE Trans. Circuits Syst.*, vol. 29, no. 6, pp. 345-354, 1982.
- [20] F. Cuesta, F. Gordillo, J. Aracil, and A. Ollero, "Stability analysis of nonlinear multivariable Takagi-Sugeno fuzzy control systems," *IEEE Trans. Fuzzy Syst.*, vol. 7, no. 5, pp. 508-520, 1999.
- [21] A.I. Mees, *Dynamics of Feedback Systems*. New York: Wiley, 1981.
- [22] *Modular Servo System MS150 Mk2 User's Guide*. Manual 150. Feedback Instruments Ltd.
- [23] A. Gelb and W.E. Vander Velde, *Multiple-Input Describing Functions and Nonlinear Systems Design*. Englewood Cliffs, NJ: Prentice-Hall, 1968.

**Manuel G. Ortega** received the industrial electrical engineering degree from the Escuela Superior de Ingenieros de

Sevilla in 1995. He is currently an Associate Professor in the Department of Systems Engineering and Automatic Control of the University of Sevilla. He has worked in various research and development projects in cooperation with industry. His current interests are in the areas of robust control and nonlinear systems. He has authored several technical papers published in international journals and conference proceedings.

**Javier Aracil** received the Ingeniero Industrial and the Doctor Ingeniero Industrial degrees from the Universidad Politecnica de Madrid, Spain, in 1965 and 1969, respectively. Since 1969 he has been Full Professor at the Escuela Superior de Ingenieros Industriales of the Universidad de Sevilla. In 1974 he was appointed Head of the Department of Automatic Control and Electronics. His research has covered a wide range of topics, all of them dealing with modeling and control of nonlinear systems, with emphasis on the application of the qualitative theory of nonlinear dynamical systems and to the study of bifurcations and chaos in electronic, socioeconomic, and control systems.

**Francisco Gordillo** received the Ingeniero Industrial and the Doctor Ingeniero Industrial degrees from the Universidad de Sevilla, Spain, in 1988 and 1994, respectively. Since 1989 he has been with the Department of Automatic Control of the Escuela Superior de Ingenieros of the Universidad de Sevilla, where he is currently an Associate Professor. His research interests include the application of the qualitative theory of dynamical systems to the stability analysis of nonlinear control systems, including fuzzy systems, with emphasis on electronic and electro-mechanical applications.

**Francisco R. Rubio** received the Industrial Electrical Engineering degree and the Doctorate from the Escuela Tecnica Superior de Ingenieros Industriales de Sevilla in 1981 and 1985, respectively. He received the CITEMA award for the best work on automation by a young engineer in 1980. He is a Professor in the Department of Systems Engineering and Automatic Control of the University of Sevilla. He has worked on various research and development projects in cooperation with industry. His current research interests are in the areas of adaptive control and robust process control. He has written the books *Advanced Control of Solar Plants* (Springer-Verlag) and *Control Adaptivo y Robusto* (Seville University). He has authored and coauthored more than 85 technical papers published in international journals and conference proceedings.